AUCTORES
Globalize your Research

Biotechnology and Bioprocessing
Medha Pandya *

Open Access

Research Article

Pelargonidin-3,5-Diglucoside found in Pomegranate Aril Acts as a Potent HIF-1α Inhibitor in in-Silico Study

Esha Joshi [1], Medha Pandya [2*], Shilpa Balar [1], Hiram Saiyed [1], Saumya Patel [1], Rakesh Rawal [1], Urja Desai [1]

[1] Gujarat University, Ahmedabad, Gujarat, India.

[2] Gyan Manjari University, Bhavnagar, Gujarat, India.

***Corresponding Author:** Medha Pandya, Gyan Manjari University, Bhavnagar, Gujarat, India.

Received date: March 27, 2023; **Accepted date:** April 04, 2023; **Published date:** April 10, 2023

Citation: Esha Joshi, Medha Pandya, Shilpa Balar, Hiram Saiyed, Saumya Patel, et al, (2023), Pelargonidin-3,5-Diglucoside found in Pomegranate Aril Acts as a Potent HIF-1α Inhibitor in in-Silico Study, *J, Biotechnology and Bioprocessing*, 4(2); DOI: 10.31579/2766-2314/096

Abstract

Hypoxia-inducible factor 1 alpha (HIF-1α) is a transcription factor that regulates the transcription of over 100 genes involved in erythropoiesis, angiogenesis, autophagy, cell survival, and energy metabolism signaling; it appears to be a potential target in cancer therapy. The aim of this study was to identify natural compounds from Naturally Occurring Plant-based Anti-cancer Compound-Activity-Target (NPACT) database with anticancer potential. Molecular docking of 1574 phytochemicals was carried out using Autodock Vina 1.1.2 using the site-specific docking method and the amino acid residue site was near Asn803 of HIF-1α. The protein-ligand complexes considered for molecular dynamics simulation were HIF1α- Bortezomib (as control), HIF 1α- Pelargonidin-3 ,5-diglucoside and HIF1α- (25S)-5-beta-spirostan-3-beta-ol-3-O-alpha-L-rhamnopyranosyl-(1->2)-[alpha-L-rhamnopyranosyl-(1->4)]-beta-D-glucopyranoside. Furthermore, ADMET evaluation for the best ligands was carried out using the pkCSM ADMET server.

Key Words: amino acid; neurons; ischemia; omega-3 polyunsaturated acids

Introduction

Hypoxia is a decrease in normal tissue oxygen tension and is a universal characteristic of solid tumors; their ability to adapt to hypoxic conditions is critical to their existence and advancement, and hence could be harnessed in cancer therapy as depicted in Figure 1 and it can arise during the avascular state of tumor, or can emerge in established tumors as a result of inadequate angiogenesis that simply delivers insufficient blood supply [1,2,3]. The rules that govern cellular responses to hypoxia are the hypoxia-inducible factors (HIFs)4. In general, higher HIF expression is linked to tumor growth and therapy resistance, which culminates in disease relapse5. HIFs are categorized into three isoforms: HIF-1, HIF-2, and HIF-36. HIF-1 is regarded to be the principal messenger for hypoxia-induced transcriptional responses and is an indiscriminate heterodimeric transcription factor that consists of two subunits: an α and β. The availability of the HIF-1α subunit, which increases under hypoxic environment, is required for HIF-1 function in tumors [3]. Oxygen-dependent post-translational modifications impact the stability, subcellular localization, and transcriptional strength of the α subunit, and thus oxygen concentration [7]. As HIF-1α regulates the transcription of over 100 genes involved in erythropoiesis, angiogenesis, autophagy, cell survival, and energy metabolism signaling; it appears to be a potential target in cancer therapy [8,9]. The main target genes of HIF-1α are LEP, NO, VEGF, LRP1, ADM, TGF-β for angiogenesis; EPO for erythropoiesis; HK1, HK2, GLUT1, GLUT3, LDHA, PKM for metabolism; IGF2, IGF-BP1, IGF-BP2, IGF-BP3, NOS2, TGF-α for cell-survival and C-MYC, ID2, IGF-2, NOS for cell-proliferation [8,9,10,51]. In normoxic conditions, HIF-1α is degraded by two pathways: (i) pVHL dependent pathway and (ii) pVHL independent pathway as shown in Figure 2. pVHL dependent pathway involves acetylation by ARD1 (Arrest Defective 1) on lysine 532 residue, hydroxylation by PHDs (Prolyl-4-Hydroxylases) on proline 402 and 564 residues, followed by acetylation and ubiquitination on lysine 532 residue; hydroxylation and ubiquitination on proline 402 and proline 564 by pVHL (von Hippel-Lindau protein) and ultimately proteosomal degradation of HIF-1α [10]. While the pVHL independent pathway involves hydroxylation on asparagine 803 by FIH-1 (Factor Inhibiting Hypoxia 1) and thereafter binding of FIH-1 with HIF-1α and hence inhibition of HIF1α and P300/CBP (CREB Binding Protein) dimerization [11].

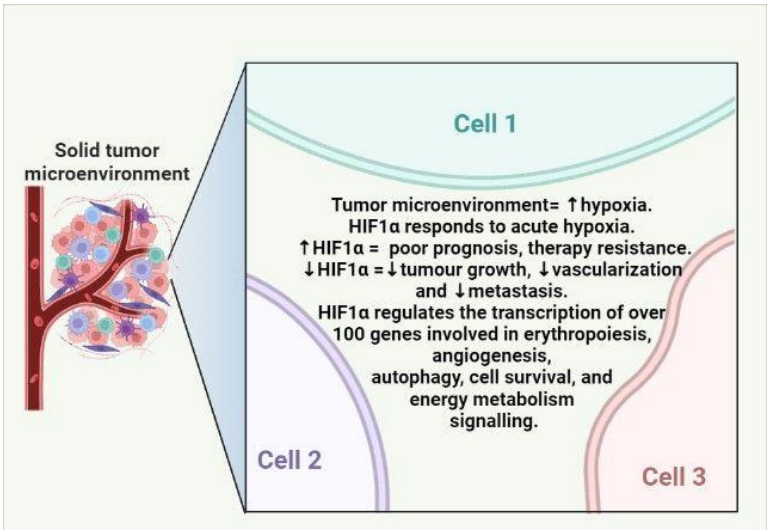

Figure 1: Hypoxia levels are very high in the tumor microenvironment. The above diagram summarizes hypoxia functions in tumor microenvironment (TME).

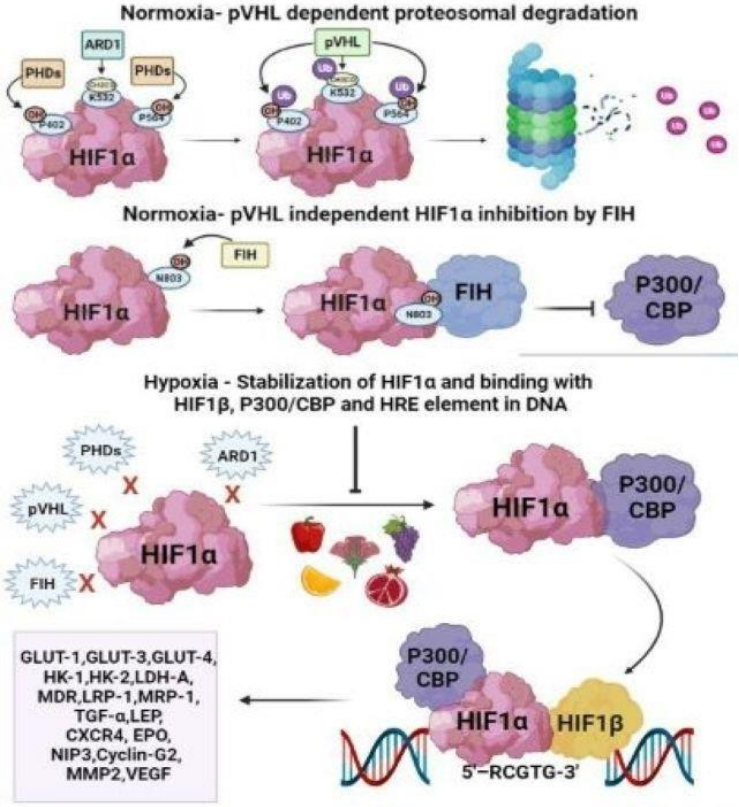

Figure 2: Above figure is modified from Joshi et al. 202351. Degradation and transcription pathway of HIF-1α in normoxia and hypoxia. In normoxic conditions HIF-1α is degraded by several factors including PHDs (PHD1, PHD2 and PHD3), ARD1, pVHL and FIH. However, in hypoxic TME none of these factors are able to degrade HIF-1α and also P300/CBP as well as HIF-1β acts as co-activators for HIF-1α transcription and thus contributes to the upregulation of down-stream genes.

As illustrated in Figure 2, during hypoxic conditions, HIF-1α and P300/CBP dimerization takes place at the asparagine 803 residue which later moves towards the nucleus and binds with HIF-1β and HRE (Hypoxia Response Element) sequence 5'-RCGTG-3' located on the DNA [10,12].

Despite significant technological breakthroughs in standard therapies, cancer remains the dominant cause of death worldwide. According to the Indian Council of Medical Research, the estimated number of people with cancer is around 2.7 million 2020, each year, new 13.9 lakhs cancer patients are registered and the number of deaths related to Cancer have risen up to 8.5 lakhs in 2020. A fundamental contributing factor to the suboptimal effectiveness of chemotherapy is the unique architectural makeup of tumors. Specifically, in the case of solid tumors, cells situated in hypoxic regions, which are commonly distal from the vasculature, experience constrained access to chemotherapeutic agents due to the atypical vascularization. And also, the MDR1 gene, which is also a target of HIF-1α, represents a

significant impediment to effective cancer treatment, as it plays a pivotal role in promoting chemoresistance of cancer cells towards various therapeutic interventions. Chemotherapy is the most efficacious strategy to combat cancer, but it still has detrimental effects. Because of the adverse effects of radiotherapy and chemotherapy, alternative cancer preventive and treatment strategies with no or few side effects are necessary. Natural products can be used as chemotherapeutic and chemo preventive agents as plants and their active constituents have been employed for therapeutic purposes since earlier civilizations. Phytochemicals are currently evolving as gold mines of potent as well as healthier medications against a wide range of life-threatening disorders [13,14,24,26].

Secondary metabolites of plants such as alkaloids possess strong anticancer activity both in-vitro and in-vivo, and can act as CDK or protein kinase inhibitors and can be transformed as novel anticancer agents [16]. A vinca alkaloid, vincristine is a mitotic inhibitor, useful in cancer chemotherapy. Liposomal vincristine has been given FDA approval for treating acute leukemias [17,18]. Polyphenol-derived natural products have gained scientific interest due to their ability to modulate various cancer hallmarks. These hallmarks are a set of distinct biological capabilities acquired by neoplastic cells that enable them to evade host defense mechanisms. Quercetin, a flavonoid, suppresses expression of anti-apoptosis protein Bcl-2 and manages the protein expression of pro-apoptosis Bax and also activates caspase-3, that initiates caspase-3 dependent mitochondrial pathway to induce apoptosis, it also inhibits mTOR phosphorylation and controls AMPK expression in leukemic cells to restrict cell development and trigger cell death [15,24].

Several phytochemicals have exhibited synergistic effects in combination with conventional chemotherapy drugs [19]. For instance, the polyphenol resveratrol, when administered in conjunction with prednisolone, has been observed to decrease the expression of MDR1 protein in cancer cells. Similarly, the flavonoids hesperidin and silibinin, when co-administered with cytarabine at a fixed dose and varied concentration, have been shown to reduce the IC50 value of cytarabine by approximately ~5.9 and ~4.5 times, respectively. This presents a promising approach for combination therapy with lower cytotoxicity [20]. Furthermore, the phytoestrogen genistein, found in soybeans, has been found to sensitize ovarian cancer cells to the chemotherapy drug cisplatin by inhibiting the NF-κB signaling pathway [21].

Phytochemicals have demonstrated the ability to enhance the bioavailability and uptake of one another. For example, (−)-epicatechin has been observed to increase the incorporation of EGCG in human lung cancer cell line PC-9. Additionally, co-administration of DHA and curcumin at the same concentrations has been shown to significantly augment the uptake of curcumin in human breast cancer SK-BR-3 cells, possibly through alterations in membrane lipid composition [22]. Secondly, in the latest trends of nanotechnology, nanotechnology-mediated delivery of small nucleotides and nucleic acids offers an effective therapeutic strategy for various cancer types [50].

Results

2.1 Homology modelling and structure validation

The quality of HIF-1α was analysed using the PROCHECK program for further structural validation. The graphical representation of the target protein's predicted tertiary structure and Ramachandran plot analysis are shown in Figure 3. The Ramachandran plot indicates that 63.1% of the residues of the modelled protein were located within the most favored region, 30.5% in additionally allowed region, and 3.4% of the residues in the disallowed region. Thus, the data suggested that the predicted model is reliable for further analysis.

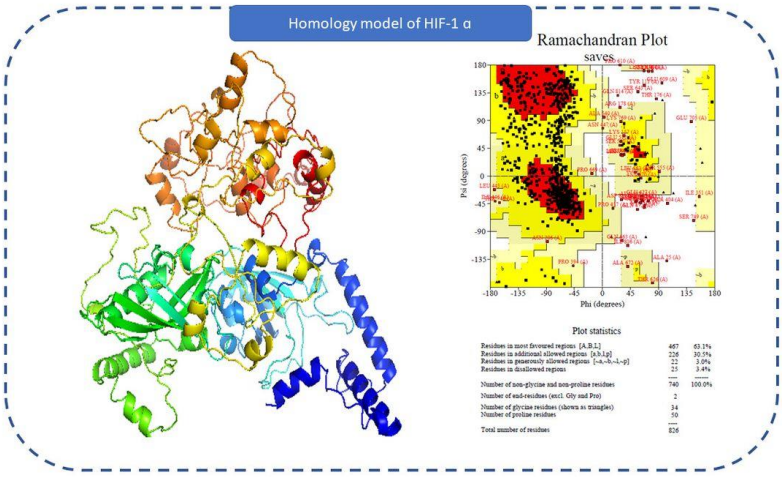

Figure 3: Homology model and Ramachandran plot of Hypoxia inducible factor-1α.

2.2 Analysis of HIF 1 α and its interaction with bortezomib

Recent researchers reported that Bortezomib (PS-341; Velcade, Cambridge, MA) is one of the functional inhibitors of HIF-1α. Bortezomib causes tumor cell death directly and has also been shown to limit tumor adaptation to hypoxia by functionally blocking HIF-1α [23]. The molecular docking of the most potent hypoxic factor HIF-1α was carried out by targeting Asn803 as a docking site for the bortezomib as control. Asn803 serves as a binding site for co-activators P300/CBP required for the transcriptional activation of HIF-1α during hypoxia. In cancer cells, hypoxic microenvironment is a hallmark thus, HIF-1α is stabilized and transcription takes place after the dimerization of HIF-1α with HIF-1β and binding of co-activators P300/CBP and HRE element on the DNA. In-silico molecular docking of HIF-1α leads to -10.8 kcal/mol binding energy with bortezomib as listed in Table 1. The molecular interaction of HIF-1α and bortezomib depicted in Figure 4 and the interacting residues in the cavity are Glu817 with H-bond interaction and Val802, Asn803, Thr796, Tyr798, Leu812, Leu813, Asn689, Val690, Cys800, Glu801 in hydrophobic interactions. Binding of bortezomib with HIF-1α shows that it binds in the co-activators binding pocket as shown in Figure 4: and can inhibit transcriptional activation of HIF-1α.

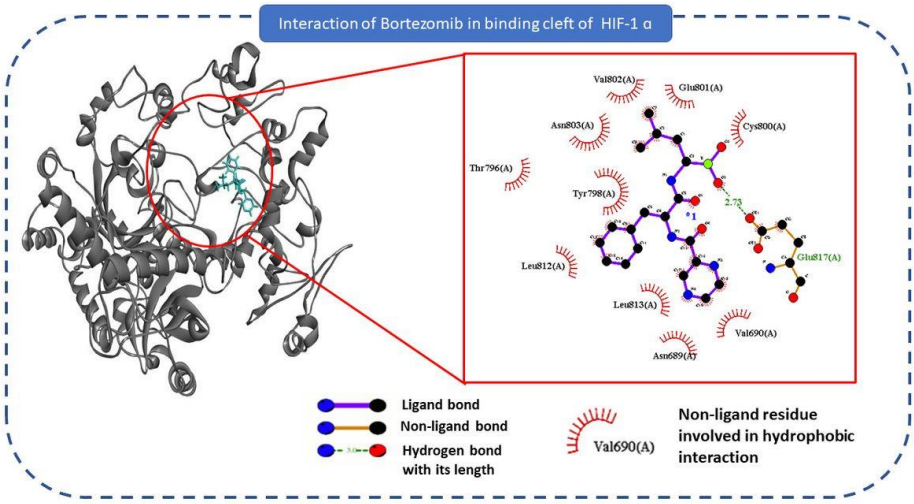

Figure 4: Interaction of Bortezomib in the binding cleft of HIF-1α shown in 3-D representation and 2-D representation (for better clarity) describing ligands interactions by formation of various H-bonds and hydrophobic interactions with protein at the active site of the protein.

2.3 Docking of HIF-1α with phytochemicals from NPACT with anti-cancer potential

The NPACT database contains natural chemicals derived from plants that have anticancer properties. Molecular docking study was carried out to evaluate all anticancer natural compounds from this database against HIF-1α. Table 1 lists the top 5 compounds with the lowest binding energies and interacting amino acid residues. The natural flavonoid pelargonidin-3,5-diglucoside reported best binding energy with HIF-1α. Pelargonidin-3,5-diglucoside forming (Figure 5) H-bonds with Val802 (3.04 Å), Ala779 (2.74 Å, 3.30 Å), Gln785 (3.31 Å), Leu783 (3.07 Å), Arg810 (2.89 Å, 2.99 Å), Ser809 (3.01 Å), Asp788 (2.97 Å), Thr798 (2.41 Å, 3.03 Å).

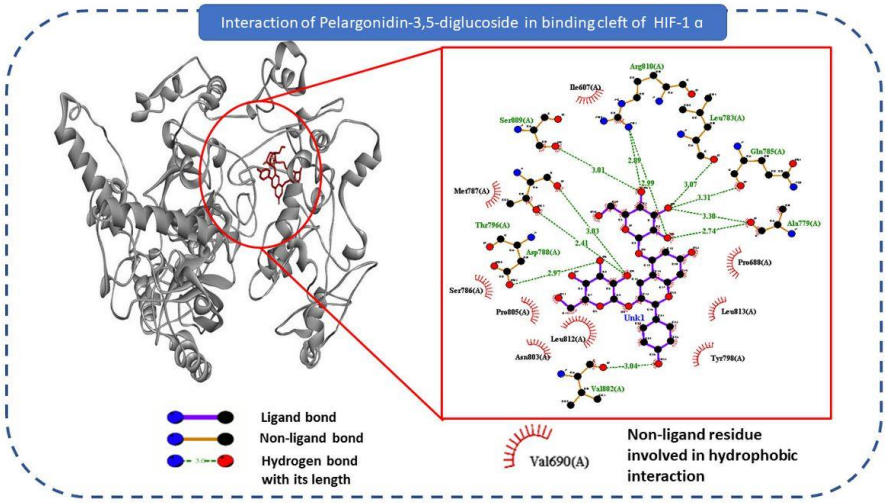

Figure 5: Interaction of Pelargonidin-3,5-diglucoside in the binding cleft of HIF-1α shown in 3-D representation and 2-D representation (for better clarity) describing ligands interactions by formation of various H-bonds and hydrophobic interactions with protein at the active site of the protein.

It forms hydrophilic interactions with Ile607, Met787, Ser786, Pro805, Leu812, Asn803, Tyr798, Leu813, Pro688. Another natural steroid is found in Asparagus officinalis, (25S)-5-beta-spirostan-3-beta-ol-3-O-alpha-L-rhamnopyranosyl-(1->2)-[alpha-L-rhamnopyranosyl-(1->4)]-beta-D-plucopyranoside yields − 11.1 with only one H-bond at Leu797 with bond length 3.15 Å and nineteen hydrophilic bonds at Tyr798, Ala804, Gln814, Leu812, Pro805, Asn803, Ala779, Asp788, Leu783, Arg810, Gln785, Ser809, Ser786, Ile607, Met787, Thr796, Glu817, Val802, Asp83. The third natural saponin named Hederagenin 3-O-beta-D-glucopyranosyl-(1->3)-alpha- L- rhamnopyranosyl-(1->2)-alpha-L- arabinopyranoside binds to HIF-1α with three H-bonds at Asn803 (2.84 Å), Ser786 (3.19 Å), Asp (3.10 Å) and ten hydrophilic bonds Glu817, Tyr798, Ser797, Leu795, Met787, Ser809, Leu812, Pro805, Thr796, Val 802. The binding energies of flavonoid Calyxins K and 7,7"-dimethyllanaraflavone is -10.6 and − 10.5 kcal/mol subsequently and the interacting residues of HIF-1 α with this two-flavonoid depicted in Table1.

Compound No.	Molecule Name	Binding Energy (kcal/mol)	Class	H- bond Interactions		Hydrophilic Interactions	
				No. of Bonds	Residues in Interaction (with bond length)	No. of Bonds	Residues in Interaction (with bond length)
Compound	Bortezomib	-10.8	Anti-cancer Drug	01	Glu817 (2.73 Å)	10	Val802, Asn803, Thr796, Tyr798, Leu812, Leu813, Asn689, Val690, Cys800, Glu801
1	Pelargonidin-3,5-diglucoside	-12	Flavonoid	11	Val802 (3.04 Å), Ala779 (2.74 Å, 3.30 Å), Gln785 (3.31 Å), Leu783 (3.07 Å), Arg810 (2.89 Å, 2.99 Å), Ser809 (3.01 Å), Asp788 (2.97 Å), Thr798 (2.41 Å, 3.03 Å)	09	Ile607, Met787, Ser786, Pro805, Leu812, Asn803, Tyr798, Leu813, Pro688
2	(25S)-5-beta-spirostan-3-beta-ol 3-O-alpha-L-rhamnopyranosyl-(1->2)-[alpha-L-rhamnopyranosyl-(1->4)]-beta-D-glucopyranoside	-11.2	Steroid	01	Leu797 (3.15 Å)	19	Tyr798, Ala804, Gln814, Leu812, Pro805, Asn803, Ala779, Asp788, Leu783, Arg810, Gln785, Ser809, Ser786, Ile607, Met787, Thr796, Glu817, Val802, Asp83
3	Hederagenin 3-O-beta-D-glucopyranosyl-(1->3)-alpha-L-rhamnopyranosyl-(1->2)-alpha-L-arabinopyranoside	-11.2	Saponin	03	Asn803 (2.84 Å), Ser786 (3.19 Å), Asp (3.10 Å)	10	Glu817, Tyr798, Ser797, Leu795, Met787, Ser809, Leu812, Pro805, Thr796, Val 802
4	Calyxins K	-10.6	Flavonoid	07	Cys800 (3.14 Å), Val802 (3.03 Å), Thr796 (2.80 Å), Ser786 (3.02 Å), Ala779 (2.98 Å), Ser797 (2.98 Å), Tyr798 (3.24 Å)	09	Glu801, Asn803, Asp788, Ser809, Val690, Leu812, Met787, Pro688, Glu817
5	7,7"-dimethyllanaraflavone	-10.5	Flavonoid	03	Tyr798 (2.89 Å), Ser786 (2.73 Å), Glu817 (3.02 Å)	12	Leu812, Ile607, Ser809, Arg810, Pro688, Leu782, Val693, Ile677, Leu783, Met787, Val690, Leu813

Table 1: Results of Molecular docking of top molecules of NPACT in interaction with HIF-1α

2.4 Molecular dynamics simulation:

To verify the molecular docking binding affinity results the molecular dynamics simulation approach has been used systematically to investigate the properties of conformational changes that result in changes in protein-ligand interactions, molecular dynamics, and protein folding. MD simulation of complex HIF-1α with Bortezomib and HIF-1α with Pelargonidin-3,5-

diglucoside were performed for 100 ns. Analysis of both the complex in context to root mean square deviation (RMSD), root mean square fluctuation (RMSF) and Radius of gyration (Rg) depicted in Figure 6.

After superimposing the receptor on its reference structure, the RMSD of the ligand's heavy atoms was determined. The resulting plots for all the protein-ligand complexes are shown in Figure 6 (a) for bortezomib and 6 (b) for pelargonidin-3,5-diglucoside. This process provides data on how the ligand moves within its binding pocket. The oscillations of bortezomib starts after 0 Å and before 2 Å and goes around 12 Å at 100 ns while for pelargonidin-3,5-diglucoside the highest peak observed is at 16 Å in the middle of 40 ns to 60 ns and that particular point of time, the alterations are not in increased amounts. The pelargonidin-3,5-diglucoside- HIF-1 α complex scale of fluctuation and the divergence between the average RMSD values acclaimed that simulation produced stable trajectories in contrast to control complex.

The functional analysis and the maximum fluctuation in this site are correlated with the root mean square fluctuation analysis (Figure 6c & d). This observed fall in the scores of specific residues indicates that they have a direct role in improving the overall stability of the bound protein complex. The RMSF value is beneficial for illustrating localized minute changes along protein chains and offers information on the dynamic behaviour of proteins in an aqueous simulated environment. The protein districts that change the most during the simulation are shown by the peaks in the diagram. N- and C-terminal protein tails are more prone to change than other regions of the protein. Alpha helices and beta strands, two protein auxiliary regions, are frequently stiffer and more inflexible than unstructured parts. The amino acid residues 350–450 showed high fluctuations in both the complexes. The radius of gyration is calculated and plotted using data collected outside the simulation cell, where each item has its own local coordinate system and no periodic borders are present. The graph for bortezomib starts at 0 ns, reaches the peak at 40 Å in between 30 ns to 40 ns. Pelargonidin-3,5-diglucoside rises at the highest peak above 33.2 Å at 0 ns and falls the lowest to 31.6 Å at 90 ns.

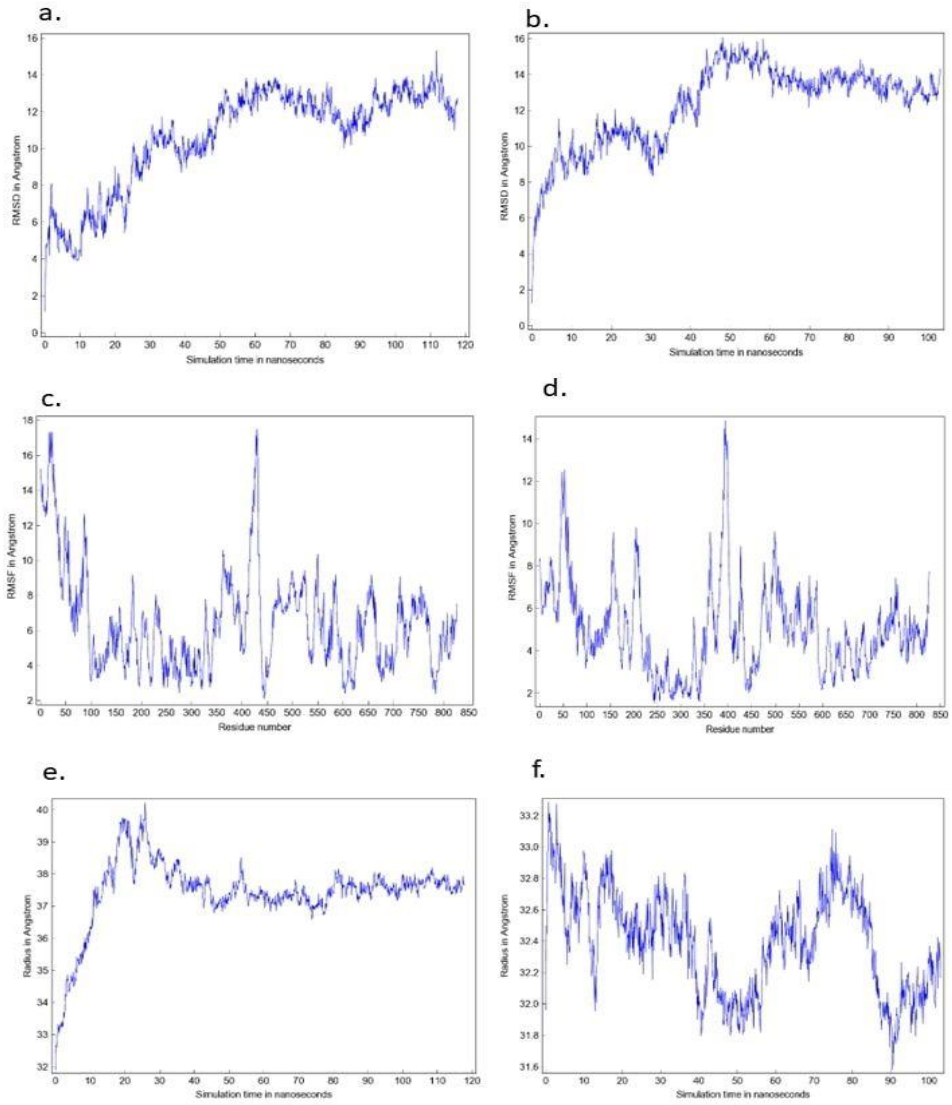

Figure 6: MD simulation trajectory results for Bortezomib (control) and Pelargonidin-3,5-diglucoside. (a) Ligand movement RMSD of Bortezomib (control) after superposing on receptor (b) Ligand movement RMSD of Pelargonidin-3,5-diglucoside (compound 1) after superposing on receptor (c) Solute Protein Nucleic Acid Residue RMSF of control (d) Solute Protein Nucleic Acid Residue RMSF of compound 1 (e)Radius of gyration of solute for Control (f) Radius of gyration of solute for compound 1.

2.5 ADMET analysis

The Table 2 summarizes the absorption, distribution, metabolism, excretion and toxicity properties of the top five docked compounds. The compounds that were studied includes- Pelargonidin-3,5-diglucoside (compound 1), (25S)-5-beta-spirostan-3-beta-ol 3-O-alpha-L-rhamnopyranosyl-(1->2)-[alpha-L-rhamnopyranosyl-(1->4)]-beta-D-glucopyranoside (compound 2), Hederagenin 3-O-beta-D-glucopyranosyl-(1->3)-alpha-L-rhamnopyranosyl-(1->2)-alpha-L-arabinopyranoside (compound 3), Calyxins K (compound 4) and 7,7"-dimethyllanaraflavone (compound 5). The main predictor of the absorption properties in in-silico ADMET analysis is the CaCO2 permeability. If a compound's Papp is greater than 8 X 10− 6 cm/s, it is said to have a high CaCO2 permeability. High CaCO2 permeability would produce projected values > 0.90 for the pkCSM predictive model. All the top five compounds have good CaCO2 permeability values as pkCSM predicted. The steady state volume distribution (VDss), for distribution parameters, is the hypothetical volume over which a drug's whole dose would need to be evenly dispersed to have the same concentration as blood plasma. Low VDss is defined as less than 0.71 L/kg (log VDss <-0.15) and high VDss is defined as more than 2.81 L/kg (log VDss > 0.45). Metabolism parameters that are included comprises of- cytochrome P450 inhibitors and CYP2D6/CYP3A4 substrate. Total clearance and renal OCT2 substrate are excretion parameters. Toxicity levels are predicted using ten parameters.

The absorption, distribution, metabolism, excretion, and toxicity properties of the top five docked compounds were summarized in Table 2. The compounds investigated were Pelargonidin-3,5-diglucoside (compound 1), (25S)-5-beta-spirostan-3-beta-ol 3-O-alpha-L-rhamnopyranosyl-(1->2)-[alpha-L-rhamnopyranosyl-(1->4)]-beta-D-glucopyranoside (compound 2), Hederagenin 3-O-beta-D-glucopyranosyl-(1->3)-alpha-L-rhamnopyranosyl-(1->2)-alpha-L-arabinopyranoside (compound 3), Calyxins K (compound 4), and 7,7"-dimethyllanaraflavone (compound 5). In silico ADMET analysis identified CaCO2 permeability as the main predictor of absorption properties. A compound is considered to have high CaCO2 permeability if its Papp value exceeds 8 x 10− 6 cm/s, resulting in projected values > 0.90 for the pkCSM predictive model. All of the top five compounds had good CaCO2 permeability values as predicted by pkCSM. The steady-state volume of distribution (VDss) is a hypothetical volume over which a drug's entire dose must be uniformly distributed to achieve the same concentration as blood plasma. A low VDss is defined as less than 0.71 L/kg (log VDss <-0.15), while a high VDss is defined as more than 2.81 L/kg (log VDss > 0.45) for distribution parameters. Metabolism parameters include cytochrome P450 inhibitors and CYP2D6/CYP3A4 substrates. Total clearance and renal OCT2 substrate are excretion parameters, while toxicity levels are predicted using ten parameters.

Molecule properties	Descriptor	Compound 1	Compound 2	Compound 3	Compound 4	Compound 5
	Molecular Weight	595.53	913.152	913.108	582.649	566.518
	LogP	-1.8505	1.7967	1.3453	6.8608	6.1597
	Rotatable Bonds	7	9	9	7	6
	Acceptors	14	16	16	8	10
	Donors	10	8	10	4	3
	Surface Area	236.739	378.101	375.575	249.284	236.352
Absorption	Water solubility (log mol/L)	-2.922	-3.033	-2.868	-3.575	-2.981
	CaCO2 permeability (log Papp in 10− 6 cm/s)	0.827	0.882	0.543	0.824	0.207
	Human Intestinal absorption (% Absorbed)	65.309	51.199	0	94.115	87.95
	Skin Permeability (log Kp)	-1.735	-1.576	-2.735	-2.389	-2.735
	P-glycoprotein substrate (Yes/No)	Yes	Yes	Yes	No	No
	P-glycoprotein I inhibitor (Yes/No)	No	Yes	No	Yes	Yes
	P-glycoprotein II inhibitor (Yes/No)	No	No	No	Yes	Yes
Distribution	VDss (human) (log L/kg)	-0.462	-0.4	-0.433	-1.244	-1.128
	Fraction unbound (human) (Fu)	0.207	0.431	0.394	0.334	0.423
	BBB permeability (log BB)	-2.503	-1.826	-1.671	-1.313	-1.824
	CNS permeability (log PS)	-6.134	-4.689	-4.89	-2.711	-3.475
Metabolism	CYP2D6 substrate (Yes/No)	No	No	No	No	No

Molecule properties	Descriptor	Compound 1	Compound 2	Compound 3	Compound 4	Compound 5
	CYP3A4 substrate (Yes/No)	No	Yes	No	No	Yes
	CYP1A2 inhibitor (Yes/No)	No	No	No	No	No
	CYP2C19 inhibitor (Yes/No)	No	No	No	Yes	No
	CYP2C9 inhibitor (Yes/No)	No	No	No	Yes	Yes
	CYP2D6 inhibitor (Yes/No)	No	No	No	No	No
	CYP3A4 inhibitor (Yes/No)	No	No	No	Yes	No
Excretion	Total Clearance (log ml/min/kg)	0.426	0.352	0.043	-0.214	0.887
	Renal OCT2 substrate (Yes/No)	No	No	No	No	No
Toxicity	AMES toxicity (Yes/No)	No	No	No	No	No
	Max. tolerated dose (human) (log mg/kg/day)	0.688	-2.51	0.079	0.32	0.375
	hERG I inhibitor (Yes/No)	No	No	No	No	No
	hERG II inhibitor (Yes/No)	Yes	Yes	No	Yes	Yes
	Oral Rat Acute Toxicity (LD50) (mol/kg)	2.526	3.085	2.567	2.423	2.684
	Oral Rat Chronic Toxicity (LOAEL) (log mg/kg bw/day)	4.453	2.845	4.93	2.027	1.957
	Hepatotoxicity	No	No	No	No	No
	Skin Sensitisation	No	No	No	No	No
	T.Pyriformis toxicity	0.285	0.285	0.285	0.285	0.285
	Minnow toxicity	9.385	7.498	6.076	-1.867	-3.278

Table 2: Results for pharmokinetic properties or ADMET analysis of the top 5 compounds

Discussion

HIF-1 α, in normal cells, is tightly regulated and maintains a balance between oxygen supply and demand by promoting angiogenesis, glycolysis, and erythropoiesis. However, in cancer cells, HIF-1α is frequently overexpressed and leads to the activation of various genes that promote tumor growth, angiogenesis, and metastasis [25]. Specifically, HIF-1α promotes glycolysis and the Warburg effect, a metabolic shift in cancer cells that favors glucose metabolism even in the presence of oxygen. This effect provides cancer cells with a survival advantage and allows them to proliferate even in hypoxic environments. HIF-1α is also involved in the regulation of genes that promote angiogenesis [26]. Moreover, HIF-1α has been implicated in the epithelial-to-mesenchymal transition, a process that enhances the invasive and metastatic potential of cancer cells. Overall, the overexpression and dysregulation of HIF-1α in cancer cells play a critical role in tumor progression and aggressiveness, making it an important target for cancer therapy [27]. On the other hand, chemotherapy and standard synthetic drugs can induce several side-effects due to their cytotoxic mechanism of action. For instance, hematological side-effects include bone marrow suppression, resulting in decreased red and white blood cell and platelet counts, which can lead to anemia, increased risk of infections, and bleeding disorders while neurological side-effects include peripheral neuropathy, cognitive dysfunction, and mood changes, which can result from the direct effect of chemotherapy on the nervous system or indirect effects, such as stress and anxiety [28]. On the contrary, the discovery of several other resistance mechanisms has not diminished the significance and prevalence of multidrug resistance (MDR) as the main cause of chemotherapy failure [49].

Hence, this gives rise to the need of treatment using a more natural way. Thus, whether the proposed work can modulate or reduce the activity of HIF-1α using phytochemicals might contribute to the forthwith research on HIF-1α. In the work described above, we molecularly docked HIF-1α with a 1574- natural compound library named NPACT and then considered the compounds with the best docking scores for molecular dynamics (MD) simulations and ADMET analysis. The very first compound, pelargonidin-3,5-diglucoside, with a dock score of -12, is abundant in pomegranate seeds and hence will be easily accessible. The second compound (25S)-5-beta-spirostan-3-beta-ol-3-O-alpha-L-rhamnopyranosyl-(1->2)-[alpha-L-rhamnopyranosyl-(1->4)]-Beta -D-Glucopyranoside is found in the Indian Ayurvedic plant Asparagus officinalis or Shatavari and will be a great option for natural cancer treatment.

Pelargonidin-3,5-diglucoside is an anthocyanin, which is a phytochemical that imparts the characteristic red, purple or blue tincture to fruits and vegetables. These pigments are known to exert several health-promoting effects, including anti-cancer properties. High concentrations of Pelargonidin-3,5-diglucoside have been identified in the fruits of Berberis vulgaris (barberry), Punica granatum (pomegranate), Fragaria ananassa (strawberry), as well as in the beans of Phaseolus vulgaris (common bean)

and kidney beans [29-31]. Pomegranate juice is recognised to be a significant source of the 3-glucosides and 3,5-diglucosides of pelargonidin, delphinidin and cyanidin [32]. There are reported studies to suggest that pelargonidin-3,5-diglucoside may have anti-cancer activity. In vitro studies have shown that it can inhibit the growth and proliferation of various cancer cell lines, including breast, colon, and liver cancer cells and also shows inhibition of HL-60 cells [33]. It has also been shown to induce apoptosis in these cancer cells, which is a crucial mechanism for preventing cancer growth and spread. While the exact mechanism of action of pelargonidin-3,5-diglucoside in cancer prevention and treatment is not fully understood, it is believed to involve the inhibition of various signaling pathways that are involved in cancer cell growth and survival. Overall, while more research is needed to fully understand the potential anti-cancer effects of pelargonidin-3,5-diglucoside, the available evidence suggests that it may be a promising natural compound for the prevention and treatment of certain types of cancer. In addition, animal studies have demonstrated that pelargonidin-3,5-diglucoside can reduce the incidence and size of tumors in mice with chemically-induced colon cancer.

The second docked compound, (25S)-5-beta-spirostan-3-beta-ol-3-O-alpha-L-rhamnopyranosyl-(1->2)-[alpha-L-rhamnopyranosyl-(1->4)]-beta-D-glucopyranoside with binding energy more than the standard inhibibitor bortezomib, is a plant steroid that can be obtained from the roots of Asparagus officinalis. Pharmacological studies on this plant have revealed its potential therapeutic effects such as anti-inflammatory, cytotoxic, antimutagenic, and antifungal properties. The root extract of Asparagus officinalis has demonstrated cytotoxic activity in various human tumor cell lines such as A2780, Eca-109, HO-8910, CNE, MGC-803, KB, and LTEP-a-2, as well as in the mouse L1210 tumor cell line [34].

Similarly, the next documented phytochemical is a saponin named ranks number three and is found in the roots of Pulsatilla koreana, which were tested for their anticancer effects in vivo using BDF1 mice exhibiting Lewis lung carcinoma (LLC) and it's in vitro cytotoxic activity against the human solid cancer cell lines SK-MEL-2, A-549, HCT15 and SK-OV-3 [35], whereas the fourth flavonoid, Calyxins K is found in the seeds of Alpinia blepharocalyx and is cytotoxic to murine colon 26-L5 carcinoma and human HT-1080 fibrosarcoma cells [36]. The last flavonoid compound is 7,7"-dimethyllanaraflavone, which is found in leaves of Ouratea hexasperma and Luxemburgia octandra enhanced growth inhibitory action in MCF-7, OVCAR-3 and NCI-H460 cell lines at 3–5 mg/ml (25% control growth) [37].

The molecular dynamics (MD) simulation outcomes indicate that the top two tested compounds exhibit comparable behavior to the FDA-approved drug bortezomib under conditions mimicking those found within the human body, including constant pressure, temperature, and pH. Consequently, these compounds should be considered for further in-vitro investigations. Additionally, the top compounds were subjected to in-silico ADMET analysis through the pkCSM server, revealing that the first and second compounds display potential as inhibitors of HIF-1α. Therefore, these compounds may represent a promising candidate for targeted therapy aimed at HIF-1α inhibition.

Materials and Methods

5.1 Homology modelling of protein and structure validation:

The amino acid sequence of HIF-1α protein was obtained from the UniProt Database (http://www.uniprot.org/) under the name HUMAN Hypoxia-inducible factor 1-alpha with sequence ID Q16665 and a total sequence length of 826 amino acid residues38. This FASTA-formatted sequence was used for additional investigation. The HIF-1α protein sequence was submitted to the I-TASSER server (https://zhanggroup.org/I-TASSER/) [39,40] for three-dimensional structure prediction using the default settings. For stereo-chemical examination of dihedral angles in modelled protein structure, the predicted models were further evaluated for correct validation and verification using UCLA- SAVES (https://saves.mbi.ucla.edu/) PROCHECK server [39]. PROCHECK examines the overall residue by residue/structural geometry as determined by the Ramachandran plot.

5.2 Molecular Docking:

The 1574 ligands were retrieved from Naturally Occurring Plant-based Anti-cancer Compound-Activity-Target (NPACT) database (https://webs.iiitd.edu.in/raghava/npact/) [41,42]. NPACT focuses solely on anti-cancer natural chemicals found primarily in plants. NPACT is unique in that it provides bioactivities of these natural chemicals against various cancer cell lines as well as their molecular targets. All compounds were optimized and processed in openable tool.

5.3 Molecular Docking and Receptor-Ligand Bond Interactions Analysis:

The homology modelled HIF-1α protein was prepared for docking analysis using MGL tools 1.5.6. The number of grid box points (x × y × z dimensions), center grid box (xyz coordinates) and grid point spacing (Å) for HIF-1α is (24 × 16× 24), 6.667, 65.123, 90.441 and 1Å. The molecular docking of 1574 phytochemicals was carried out in Autodock Vina 1.1.243 using the site-specific docking method and the amino acid residue site was near Asn803 of HIF-1α. Asn803 was selected as a target residue because it allows the binding of HIF-1α to its co-activators CBP/P300 in hypoxic conditions and further promotes transcription. Food and Drugs Administration (FDA) approved HIF-1α inhibitor Bortezomib (PubChem id.: 387447) [44] was taken as control. The binding postures were classified and evaluated based on their binding affinities. To perform protein-ligand binding site analysis, the discovery studio tool was utilized. The best 10 compounds with high binding energy obtained after molecular docking were then analysed for receptor-ligand bond interactions in Biovia Discovery Studio Visualiser [41]. The bond interactions studied included- van der Waals, conventional hydrogen bonds, carbon-hydrogen bonds, alkyl bonds, pi- alkyl bonds, unfavorable acceptor-acceptor, unfavorable donor-donor, pi-anion, pi-sigma, pi-sulphur as well as hydrogen donors and acceptors.

5.4 Molecular dynamics (MD) simulation:

YASARA was used to simulate the molecular dynamics of docked protein-ligand complexes. For MD simulations, the bound protein-ligand complexes HIF1α-Bortezomib (as the control) and HIF1α-Pelargonidin-3,5-diglucoside. In the first instance, they were all energy-minimized to prevent structural instability throughout simulations of dynamics lasting 100 nanoseconds. For simulations employing the YASARA Structure, the AMBER14 force field and TIP3P (transferable intermolecular potential with three points) water model was used. The NPT group was chosen and number of atoms, pressure, and temperature were kept constant. The protein-ligand system was neutralized by adding counter-ions (0.9% NaCl), adjusting the solvent density to 0.997g/l, the pH to 7.4, the temperature to 298 K (Berendsen thermostat), and the pressure to 1 bar (Berendsen barostat). The periodic borders of the simulation cell were turned on, and the steepest gradient energy minimization was run 100 times. Harmonic limitations were adjusted during the equilibration stage. Long-range Coulomb electrostatics was invoked using the particle mesh Ewald approach [45,46].

5.5 ADMET analysis:

Compounds for Absorption, Distribution, Metabolism, Excretion and Toxicity (ADMET) evaluation were selected on the basis of their highest binding energy and molecular dynamics simulation results. ADMET analysis was performed using the pkCSM web-server47,48. pkCSM predicts pharmacokinetic properties of compounds, which relies on graph-based signatures. Smiles format of compounds of interest were retrieved from the PubChem database and were processed for the ADMET results. Thirty predictors were used by pkCSM, and were split into five main classes: absorption (seven predictors), distribution (four predictors), metabolism (seven predictors), excretion (two predictors), and toxicity (ten predictors) [48].

Declarations

Data Availability Statement:

This article has all the data that was created or analysed during this investigation (and its Supplementary Information files).

Acknowledgements:

EJ is thankful to Scheme of Developing High quality research (SHODH), Education department, Government of Gujarat, India for availing the student support fellowship. All authors would like to thank Department of Zoology, Biomedical Technology, Human Genetics & Wildlife Conservation and Department of Botany, Bioinformatics and Climate Change Impacts Management, School of Sciences at Gujarat University for allowing access to the advance instrumentation and the bioinformatics research facilities. We are also thankful to the Department of Life Sciences, Maharaja Krishna Kumar Sinhji Bhavnagar University, Bhavnagar and also to Department of Biochemistry and Forensic Science, Gujarat University, Ahmedabad, Gujarat.

Funding Information:

No specified grant for the above-mentioned research was provided by funding organizations in the public, private, or non-profit sectors.

Author contributions:

E.J. and M.P. wrote the manuscript, performed experiments, prepared figures and tables. S.B. helped in preparing the manuscript. U.D., M.P. and S.P. conceptualized the idea, R.M.R., S.P. M.P. and U.D. critically proofread the manuscript.

Corresponding Author:

Correspondence to Dr. Urja Desai and Dr. Medha Pandya.

Competing Interests:

All the authors of the provided manuscript declare no conflicts of interest.

References

1. Hong, S.-S., Lee, H. & on Kim, K.-W. (2004). H IF-1α: a Valid Therapeutic Target for Tumor Therapy. *Cancer Research and Treatment* vol. 36.
2. Carmeliet P, Jain RK. (2000). Angiogenesis in cancer and other diseases. *Nature*. 407(6801):249-257.
3. Burslem, G. M., Kyle, H. F., Nelson, A., Edwards, T. A. & Wilson, A. J. (2017). Hypoxia inducible factor (HIF) as a model for studying inhibition of protein-protein interactions. Chemical Science vol. 8 4188–4202.
4. Deynoux, M., Sunter, N., Hérault, O. & Mazurier, F. (2016). Hypoxia and hypoxia-inducible factors in leukemias. *Frontiers in Oncology* vol. 6.
5. Mimeault, M. & Batra, S. K. (2013). Hypoxia-inducing factors as master regulators of stemness properties and altered metabolism of cancer- and metastasis-initiating cells. *Journal of Cellular and Molecular Medicine* 17, 30–54.
6. Nordgren, I. K. & Tavassoli, A. (2011). Targeting tumour angiogenesis with small molecule inhibitors of hypoxia inducible factor. *Chemical Society Reviews* 40, 4307–4317.
7. Semenza, G. L. (2003). Targeting HIF-1 for cancer therapy. *Nature Reviews Cancer* vol. 3 721–732.
8. Kaelin, W. G. & Ratcliffe, P. J. (2008). Oxygen Sensing by Metazoans: The Central Role of the HIF Hydroxylase Pathway. *Molecular Cell* vol. 30 393–402.
9. Rouault-Pierre, K., Hamilton, A. & Bonnet, D. (2016). Effect of hypoxia-inducible factors in normal and leukemic stem cell regulation and their potential therapeutic impact. *Expert Opinion on Biological Therapy* vol. 16 463–476.
10. Masoud, G. N. & Li, W. (2015). HIF-1α pathway: Role, regulation and intervention for cancer therapy. *Acta Pharmaceutica Sinica* B vol. 5 378–389.
11. Lee, H. J. et al. (2019). Role of HIF1α regulatory factors in stem cells. *International Journal of Stem Cells* vol. 12 8–20.
12. Gaspar, J. M. & Velloso, L. A. (2018). Hypoxia inducible factor as a central regulator of metabolism ⇓ implications for the development of obesity. *Frontiers in Neuroscience* vol. 12.
13. Dutt, R., Garg, V., Khatri, N. & Madan, A. K. (2018). Phytochemicals in Anticancer Drug Development. *Anticancer Agents Med Chem* 19, 172–183.
14. Usman, M. et al. (2022). Exploring the Phytochemicals and Anti-Cancer Potential of the Members of Fabaceae Family: A Comprehensive Review. *Molecules*, Vol. 27, Page 3863 27, 3863.
15. Agustini, S. M., Utomo, D. H., Rifa'i, M., Haryana, S. M. & Widjajanto, E. (2019). An in-silico approach toward wheatgrass extract-induced apoptosis of human acute myeloid leukemia cells. *Drug Invention Today* 12.
16. Tao, H. et al. (2020). Alkaloids as Anticancer Agents: A Review of Chinese Patents in Recent 5 Years. *Recent Pat Anticancer Drug Discov* 15.
17. Taher, M., Nyeem, M., … M. B.-I. J. P. N. (2017), undefined. Vinca alkaloid-the second most used alkaloid for cancer treatment-A review. 2, 723–727.
18. Martino, E. et al. (2018). Vinca alkaloids and analogues as anti-cancer agents: Looking back, peering ahead. *Bioorganic and Medicinal Chemistry Letters* vol. 28.
19. Briguglio, G. et al. (2020). Polyphenols in cancer prevention: new insights (Review). *Int J Funct Nutr* 1.
20. Desai, U. et al. (2015). Enhancement of the cytotoxic effects of Cytarabine in synergism with Hesperidin and Silibinin in Acute Myeloid Leukemia: An in-vitro approach. *J Cancer Res Ther* 11.
21. Sun, C. Y., Zhang, Q. Y., Zheng, G. J. & Feng, B. (2019). Phytochemicals: Current strategy to sensitize cancer cells to cisplatin. *Biomedicine & Pharmacotherapy* 110, 518–527.
22. Zhang, L., Virgous, C. & Si, H. (2019). Synergistic anti-inflammatory effects and mechanisms of combined phytochemicals. *Journal of Nutritional Biochemistry* 69, 19–30.
23. Onnis, B., Rapisarda, A. & Melillo, G. (2009). Development of HIF-1 inhibitors for cancer therapy. *Journal of Cellular and Molecular Medicine* vol. 13 2780–2786.
24. Goel, H. et al. (2023). Unraveling the therapeutic potential of natural products in the prevention and treatment of leukemia. *Biomedicine and Pharmacotherapy* 160.
25. Cimmino, F. et al. (2019). HIF-1 transcription activity: HIF1A driven response in normoxia and in hypoxia. *BMC Med Genet* 20, 1–15.
26. Carolina Belisario, D. et al. Hypoxia dictates metabolic rewiring of tumors: implications for chemoresistance.
27. Fraga, A. et al. (2014). The HIF1A functional genetic polymorphism at locus +1772 associates with progression to metastatic prostate cancer and refractoriness to hormonal castration. *Eur J Cancer* 50, 359–365.
28. Schirrmacher, V. (2019). From chemotherapy to biological therapy: A review of novel concepts to reduce the side effects of systemic cancer treatment (Review). *Int J Oncol* 54, 407–419.
29. Yang, Q. Q., Gan, R. Y., Ge, Y. Y., Zhang, D. & Corke, H. (2018). Polyphenols in Common Beans (Phaseolus vulgaris L.): Chemistry, Analysis, and Factors Affecting Composition. *Compr Rev Food Sci Food Saf* 17, 1518–1539.
30. Giusti, M. M. & Wrolstad, R. E. (2003). Acylated anthocyanins from edible sources and their applications in food systems. *Biochem Eng J* 14, 217–225.

31. Sharifi, A., Niakousari, M., Mortazavi, S. A. & Elhamirad, A. H. (2019). High-pressure CO 2 extraction of bioactive compounds of barberry fruit (Berberis vulgaris): process optimization and compounds characterization. *Journal of Food Measurement and Characterization* 13, 1139–1146.
32. Paul, A., Banerjee, K., Goon, A. & Saha, S. (2018). Chemo-profiling of anthocyanins and fatty acids present in pomegranate aril and seed grown in Indian condition and its bioaccessibility study. *J Food Sci Technol* 55, 2488–2496.
33. Dreiseitel, A., Schreier, P., Oehme, A., … S. L.-B. (2008), undefined. Inhibition of proteasome activity by anthocyanins and anthocyanidins. *Elsevier*.
34. Huang, X. F., Lin, Y. Y. & Kong, L. Y. (2008). Steroids from the roots of Asparagus officinalis and their cytotoxic activity. *J Integr Plant Biol* 50, 717–722.
35. Bang, S., Lee, J., Song, G., … D. K.-C. (2005), undefined. Antitumor activity of Pulsatilla Korean saponins and their structure–activity relationship.
36. Tezuka, Y., Gewali, M. B., Ali, M. S., Banskota, A. H. & Kadota, S. Eleven, (2001). novel diarylheptanoids and two unusual diarylheptanoid derivatives from the seeds of Alpinia blepharocalyx. *J Nat Prod* 64, 208–213.
37. Daniel, J. de S., Alves, C., … I. G.-I. J. (2007), undefined. Antitumor activity of bioflavonoids from Ouratea and Luxemburgia on human cancer cell lines.
38. Bateman, A. et al. (2017). UniProt: The universal protein knowledgebase. *Nucleic Acids Research* 45, D158–D169.
39. Pandya, M. et al. (2015). Structural and Functional Analysis of Af9-Mll Oncogenic Fusion Protein Using Homology Modeling and Simulation Based Approach. SARS-CoV-2 View Project Molecular targeting of GC binding transcription factor View project. Article in *International Journal of Pharmacy and Pharmaceutical Sciences* vol. 13.
40. Yang, J. et al. (2014). The I-TASSER suite: Protein structure and function prediction. Nature Methods vol. 12 7–8.
41. Pandya, H. et al. (2020). Analyzing the role of phytochemicals in targeting drug transporter protein ABCC6 using molecular docking and molecular dynamics simulations. International Journal of Pharmaceutical Sciences and Drug Research 275–281.
42. Mangal, M., Sagar, P., Singh, H., Raghava, G. P. S. & Agarwal, S. M. (2013). NPACT: Naturally occurring plant-based anti-cancer compound-activity-target database. *Nucleic Acids Research* 41.
43. Pandya, M. et al. (2016). Unravelling Vitamin B12 as a potential inhibitor against SARS-CoV-2: A computational approach. Informatics in Medicine Unlocked 30, 100951 (2022).
44. Kim, S. et al. PubChem substance and compound databases. *Nucleic Acids Research* 44, D1202–D1213.
45. Pandya, P. N. et al. (2020). Identification of promising compounds from curry tree with cyclooxygenase inhibitory potential using a combination of machine learning, molecular docking, dynamics simulations and binding free energy calculations. *Molecular Simulation* 46, 812–822.
46. Krieger, E. & Vriend, G. (2015). New ways to boost molecular dynamics simulations. *Journal of Computational Chemistry*, 36, 996–1007.
47. Rao, P. et al. (2022). Identifying structural–functional analogue of GRL0617, the only well-established inhibitor for papain-like protease (PLpro) of SARS-CoV2 from the pool of fungal metabolites using docking and molecular dynamics simulation. *Molecular Diversity*, 26, 309–329.
48. Pires, D. E. V., Blundell, T. L. & Ascher, D. B. (2015). pkCSM: Predicting small-molecule pharmacokinetic and toxicity properties using graph-based signatures. *Journal of Medicinal Chemistry*, 58, 4066–4072.
49. Desai, U., Pandya, M., Saiyed, H. & Rawal, R. (2023). Modulation of drug resistance in leukemia using phytochemicals: an in-silico, in-vitro, and in-vivo approach. *Recent Frontiers of Phytochemicals*, 583–599.
50. Pandya, M., Jani, S., Dave, V. & Rawal, R. (2020). Nano informatics: An Emerging Trend in Cancer Therapeutics. *Nanobiotechnology*, 135–162.
51. Joshi, E., Pandya, M. & Desai, U. (2023). Current Drugs and Their Therapeutic Targets for Hypoxia-inducible Factors in Cancer. *Curr Protein Pept Sci*, 24.

DOI: 10.31579/2766-2314/96